

Journal of Materials Chemistry A

Accepted Manuscript



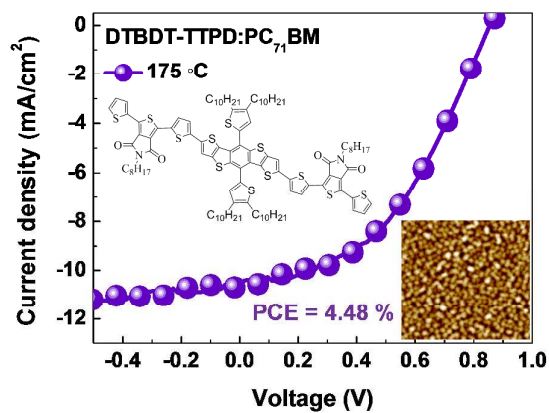
This is an *Accepted Manuscript*, which has been through the Royal Society of Chemistry peer review process and has been accepted for publication.

Accepted Manuscripts are published online shortly after acceptance, before technical editing, formatting and proof reading. Using this free service, authors can make their results available to the community, in citable form, before we publish the edited article. We will replace this *Accepted Manuscript* with the edited and formatted *Advance Article* as soon as it is available.

You can find more information about *Accepted Manuscripts* in the [Information for Authors](#).

Please note that technical editing may introduce minor changes to the text and/or graphics, which may alter content. The journal's standard [Terms & Conditions](#) and the [Ethical guidelines](#) still apply. In no event shall the Royal Society of Chemistry be held responsible for any errors or omissions in this *Accepted Manuscript* or any consequences arising from the use of any information it contains.

GRAPHICAL ABSTRACT



We designed and synthesized a dithienobenzodithiophene-based molecule with a planar molecular geometry, **DTBDT-TTPD**. It showed low band gap, deep HOMO level and their photovoltaic characteristics with power conversion efficiency as high as 4.48%.

DTBDT-TTPD: A new dithienobenzodithiophene-based small molecule for use in efficient photovoltaic devices

Ye Rim Cheon,^{a‡} Yu Jin Kim,^{b‡} Jang Yeol Back,^c Tae kyu An,^b Chan Eon Park^{b*} and Yun-Hi Kim^{a*}

^aDepartment of Chemistry & ERI, Gyeongsang National University, Jin-ju, 660-701, Republic of Korea

^bPOSTECH Organic Electronics Laboratory, Department of Chemical Engineering, Pohang University of Science and Technology, Pohang, 790-784, Republic of Korea

^cSchool of Materials Science & ERI, Gyeongsang National University, Jin-ju, 660-701, Republic of Korea

*Corresponding Authors:

1. Prof. Yun-Hi Kim

Department of Chemistry & Research Institute of Natural Science,

Gyeongsang National University,

Jin-ju, 660-701, Republic of Korea

Email: ykim@gnu.ac.kr

2. Prof. Chan Eon Park

POSTECH Organic Electronics Laboratory,

Department of Chemical Engineering,

Pohang University of Science and Technology,

Pohang, 790-784, Republic of Korea

Email: cep@postech.ac.kr

Correspondence to: Yun-Hi Kim (E-mail: ykim@gnu.ac.kr)

‡ Ye Rim Cheon and Yu Jin Kim contributed equally to this work.

Abstract

We designed and synthesized a dithienobenzodithiophene (DTBDT)-based molecule with a planar molecular geometry, **DTBDT-TTPD**, for the fabrication of solution-processable organic solar cells (OSCs). **DTBDT-TTPD** exhibited both a low optical band gap of 1.88 eV and a low-lying highest occupied molecular orbital (HOMO) energy level of -5.61 eV, indicating that **DTBDT-TTPD** is a promising electron donor for use in OSCs. OSCs prepared with **DTBDT-TTPD** as the electron donor and [6,6]-phenyl-C₇₁-butyric acid methyl ester (PC₇₁BM) as the electron acceptor were fabricated. An optimized power conversion efficiency of 4.98% with a high short circuit current of 10.6 mA/cm² was achieved after finely tuning the morphology through an annealing step. These results indicate that **DTBDT-TTPD** is an effective compound for producing very promising characteristics in small molecule solar cell devices.

Keywords

Organic solar cell, Small molecule, Dithienobenzodithiophene, Planar conformation, Power conversion efficiency

Introduction

The recent surge of enthusiasm in bulk-heterojunction (BHJ) organic solar cells (OSCs) has been driven by the goal of fabricating flexible and light-weight solar cells via facile, low-cost solution processing techniques.¹⁻² The power conversion efficiencies (PCEs) of OSCs have improved rapidly, mainly due to the development of a variety of high-performance donor polymers with near-ideal optical and electronic properties. Small molecule organic solar cells (SMOSCs) have also received significant attention because they are easily synthesized and purified, yield well-defined structures, offer good batch-to batch reproducibility, and provide reproducible solar cell performances.³⁻⁵ The PCEs of SMOSCs have thus far reached record values of ~10%.⁶

Several strategies for designing organic donors that may be used in high-performance OSCs have been established. These strategies involve (1) forming a conjugated donor–acceptor (D–A) molecular backbone to achieve broad and strong light absorption bands in the visible and near-infrared regions;⁷⁻⁸ or (2) incorporating planar molecular structures that pack closely to form crystalline structures, enhance the charge carrier mobility, and yield a large short-circuit current (J_{SC}).⁹⁻¹¹

These design ideas were used to synthesize a novel small molecule, 2,7-bis(1,3-di(thiophenyl)-5-octyl-4H-thieno[3,4-c]pyrrole-4,6(5H)-dione)-5,10-bis(4,5 didecylthiophen-2-yl)benzo[1,2-b:4,5-b']dithieno[3,2-b] thiophene (**DTBDT-TTPD**). This compound was designed to have an A-D-A alternating framework comprising dithienobenzodithiophene (DTBDT) as the core donor unit and thiophene-bridged thienopyrroledione (TPD) acceptor arm units. The DTBDT unit is a linearly fused derivative of benzodithiophene, with an enlarged planar area that can enhance the structural ordering of the polymers, thereby introducing superior intermolecular charge transport properties.¹²⁻¹³ The incorporation of DTBDT derivatives into the material structure offered a flexible way to fine-tune the

optoelectronic properties of the corresponding molecules.¹⁴ Hence, DTBDT derivatives have been widely used as building blocks in conjugated molecules for use in high-performance organic field effect transistors (OFET) and polymer solar cells. Applications of DTBDT derivatives in SMOSC materials, on the other hand, have not been extensively reported. Our group described the preparation of a semiconducting copolymer with DTBDT and benzothiadiazole moieties. The OFET produced using this copolymer displayed an impressive hole mobility of up to $0.55 \text{ cm}^2 \text{ V}^{-1} \text{ s}^{-1}$.¹⁵ Over the course of this work, Hou and co-workers reported the performances of a D–A type copolymer based on a thiophene-substituted DTBDT donor unit and a bis(trimethylstannane) acceptor unit, with a PCE of up to 7.8% in polymer solar cells.¹⁶

Thieno[3,4-*c*]pyrrole-4,6-dione (TPD) has a relatively simple, compact, and planar structure that could promote electron delocalization upon incorporation into various conjugated molecules.¹⁷⁻¹⁸ This property suggested that the moiety could promote intrachain and interchain interactions along and between coplanar molecular structures, and its relatively strong electron-withdrawing effects should, therefore, reduce the band gap in conjugated compounds.¹⁹

DTBDT-TTPD, designed according to the above molecular design strategy, displayed a small optical band gap, a low HOMO level, and a relatively high hole mobility, which provided a promising photovoltaic performance as high as 4.98%. These results suggested that **DTBDT-TTPD** could be an effective compound for producing small molecule solar cell devices with good characteristics.

Results and discussion

Synthesis and thermal properties

DTBDT-TTPD was synthesized according to Scheme 1. **DTBDT-TTPD** was synthesized

by a Stille coupling reaction of 2,7-bis(trimethylstannyl)-5,10-bis(4,5-didecylthiophen-2-yl)benzo[1,2-b:4,5-b']dithieno[3,2-b]thiophene and 1-(5-bromothiophen-2-yl)-5-octyl-3-(thiophen-2-yl)-4H-thieno[3,4-c]pyrrole-4,6(5H)-dione. The obtained compound was characterized by H-NMR, ^{13}C -NMR, and mass spectroscopy. The **DTBDT-TTPD** molecule exhibited excellent solubility in dichlorobenzene, chlorobenzene, and chloroform due to the presence of bulky alkyl side groups. The thermal properties of **DTBDT-TTPD** were investigated by thermogravimetric analysis (TGA) (Fig. 1a) and differential scanning calorimetry (DSC) (Fig. 1b). The TGA profiles revealed that the decomposition temperature (T_d , at a 5% weight loss) of **DTBDT-TTPD** was 390°C , indicating that the molecule displayed excellent thermal stability and was, thus, suitable for OSC applications.²⁰ The DSC heating trace for **DTBDT-TTPD** exhibited an endothermic peak at 97°C . During the cooling process, a similar exothermic peak was observed at 90°C and was attributed to the alkyl side chain melting in the **DTBDT-TTPD** molecule.

Optical properties

The UV-vis absorption spectra of the DTBDT-based molecules in solution or in the solid thin film state are shown in Fig. 2a. The absorption data are summarized in Table 1. **DTBDT-TTPD** displayed absorption profiles that were consistent with the intramolecular charge transfer (ICT) band typical of these groups, in both the solution and thin film states. In a dilute chloroform solution, **DTBDT-TTPD** displayed an absorption profile between 400 and 600 nm with two maximal absorption peaks (λ_{max}) at 498 nm and 524 nm. Compared to the absorption bands observed in solution, the bands in the film state were broad, and λ_{max} was significantly red-shifted to 577 nm due to strong intermolecular overlap in the condensed state.²¹ The optical bandgap (E_g^{opt}) calculated from the film absorption edge was 1.88 eV.

The PL spectra of the spin-cast films prepared using pure **DTBDT-TTPD** or a 1:2 (w/w)

blend of the small molecules and PC₇₁BM were examined to characterize the charge transfer properties of these polymers (Fig. 2b). **DTBDT-TTPD** showed a strong PL emission band with a maximum at 641 nm. The addition of PC₇₁BM nearly completely quenched the emission band, suggesting efficient photoinduced charge transfer from the small molecule to the PCBM.²²

Figure 2c shows the spectral shift and the increase in absorption intensity upon annealing the **DTBDT-TTPD**:PC₇₁BM films at various temperatures. The blended film absorbed photons across the full spectrum from 300 to 800 nm, suggesting a high light-harvesting ability when used as an active layer. A comparison to the absorption spectrum of the pure **DTBDT-TTPD** film indicated that the absorption band between 350 and 400 nm resulted mainly from the PC₇₁BM groups.²³ The blend film annealed at 175°C displayed the largest spectral changes relative to the unannealed film. The film absorption peak was red-shifted by 8 nm, to 578 nm. This shift reduced the absorbed energy, and a new structure emerged on the absorption peak associated with this transition upon thermal annealing, indicating that the **DTBDT-TTPD** molecules interacted strongly and improved the local structural order compared with films processed without annealing.²⁴

Electrochemical properties

Cyclic voltammetry was carried out to investigate the oxidative and reductive behaviors in a **DTBDT-TTPD** film mounted on a Pt electrode and examined at a scan rate of 50 mV/s. Figure 3a shows the cyclic voltammograms of **DTBDT-TTPD** films. The data are summarized in detail in Table 1. The highest occupied molecular orbital (HOMO) and lowest unoccupied molecular orbital (LUMO) energy levels were calculated using the equations:

$$E_{\text{HOMO}} = -(E_{\text{onset}}^{\text{ox}} - \text{ferrocene}_{\text{onset}}) - 4.8 \text{ eV},$$

$$E_{\text{LUMO}} = -(E_{\text{onset}}^{\text{red}} - \text{ferrocene}_{\text{onset}}) - 4.8 \text{ eV},$$

where $E_{\text{onset}}^{\text{ox}}$ and $E_{\text{onset}}^{\text{red}}$ are the onsets of the oxidation and reduction potential, respectively. Ferrocene_{onset} is the onset oxidation potential of ferrocene (0.44 eV), which was used as a reference.²⁵ The $E_{\text{onset}}^{\text{ox}}$ and $E_{\text{onset}}^{\text{red}}$ of **DTBDT-TTPD** were 1.25 and -0.81 V vs. Ag/AgCl, respectively, and the corresponding HOMO and LUMO energy levels were estimated to be -5.61 eV and -3.55 eV.

Certainly, the synthesized small molecule provided relatively low HOMO energy level that was suitable for ensuring a high V_{OC} in small molecule solar cell applications.²⁶ The LUMO energy level was about 0.36 eV above the LUMO (-3.91 eV) of the PC₇₁BM n-type acceptor, generating a driving force for energetically favorable electron transfer (see Fig. 3b).²⁷

The oxidative and reductive properties of **DTBDT-TTPD** were explored by examining the geometry and electronic structure of **DTBDT-TTPD** using Density Functional Theory. Gaussian 09 using b3lyp 6-311 G ** basis was used for the full geometry optimization calculation. Methyl alkyl groups were used in place of the long alkyl substituents to limit the computation time. The geometry and the HOMO and the LUMO surface plots of the ground state optimized structures are illustrated in Fig. S2. The HOMO was localized predominantly over the DTBDT core, whereas the LUMO contained both thiophene and TPD character. The calculated HOMO and LUMO energies of the ground state optimized geometry of the **DTBDT-TTPD** moiety were -5.25 eV and -2.74 eV, respectively, and the band gap was determined to be 2.51 eV.

Solar Cell Device Performance

The photovoltaic properties of **DTBDT-TTPD** were investigated by fabricating bulk heterojunction solar cells having the conventional structure, ITO/PEDOT:PSS/**DTBDT-TTPD**:PC₇₁BM/LiF/Al. Device optimization involved finely adjusting the blend ratios, material concentrations, and active layer thickness. The photovoltaic data are listed in detail

in the Supplementary Information. The blend ratio significantly influenced the device performance; therefore, we carefully tuned the small molecule:PC₇₁BM blend ratio from 1:1 to 1:4, 2:1, 3:1 and 4:1 (w/w) using a concentration of 40 mg/mL in chloroform (CF). An active layer with a weight ratio of 1:2 (w/w) displayed the best performance, with an open-circuit voltage (V_{oc}) of 0.68 V, a short-circuit current (J_{sc}) of 4.9 mA cm⁻², a fill factor (FF) of 48.4%, and a PCE of 1.61%. The material concentration was adjusted to provide a maximum PCE of 3.10% at 20 mg/mL. The 1:2 (w/w) blend composition at a solution concentration of 20 mg was, therefore, fixed for all further device optimization studies of the active layer thickness or thermal annealing. Optimizing the active layer thickness remarkably improved the J_{sc} by 0.1–1 mA cm⁻² and the FF by 0.5–5. The devices exhibited much higher PCEs of 3.95%, with a V_{oc} of 0.86 V, a J_{sc} of 8.4 mA cm⁻², and a FF of 54.8% at a thickness of 85 nm. Lastly, post-treatments involving thermal annealing were investigated as a means for further enhancing the device performance. Thermal annealing has been proven to be an efficient and easy method for improving the morphologies of active films. We identified an optimal annealing temperature that enhanced the device performances. Figure 4a shows the photocurrent density–voltage curves under AM 1.5G illumination at 100 mW cm⁻². The corresponding performance parameters are summarized in Table 2. All devices achieved relatively high V_{oc} values exceeding 0.85 V, consistent with the presence of a deep HOMO energy level (–5.61 eV).²⁶ The device performances, and the J_{sc} values in particular, changed dramatically after thermal annealing (at 100–200°C). The photovoltaic cell that had been thermally annealed at 175°C exhibited the highest PCE, 4.98% (V_{oc} = 0.85 V, J_{sc} = 10.6 mA cm⁻², and FF = 56.0%). The change in the PCE mainly arose from the improved J_{sc} (which increased from 8.4 to 10.6 mW cm⁻²) and the changes in the film morphology and nanostructural order, as discussed further below. J_{sc} depended strongly on the number of

excitons generated in the photoactive layers²⁸ and the photoresponse (conversion of the input photons to a photocurrent).²⁹ The thermally annealed blend films absorbed a greater fraction of incident light than the as-cast films. Annealing temperatures as high as 175°C provided much stronger light absorption coefficients (see Fig. 2c), which most likely increased exciton and charge generation in the devices that were submitted to thermal annealing. Moreover, the photoresponse, as measured by the external quantum efficiency (EQE), showed a large increase over the entire wavelength range after annealing. The EQE spectrum for the optimized film annealed at 175°C displayed a peak EQE exceeding 67% at 538 nm and a broad photoresponse from 300 nm to 700 nm. By contrast, the EQE spectrum of the device prepared without thermal annealing exceeded 51% at 530 nm (Fig. 4b). The enhanced EQE spectrum of the **DTBDT-TTPD** cells was attributed to greater conversion of incident photons into a photocurrent at all absorption wavelengths, consistent with the higher observed circuit current.³⁰

Morphological Properties

The mechanism underlying the improved device performances was investigated by characterizing the effects of thermal annealing on the surface morphology of the active layer. Figure 5 shows the height images obtained by atomic force microscopy (AFM) from the **DTBDT-TTPD:PC₇₁BM** blended films annealed at different temperatures. The blend film prepared without thermal annealing presented a relatively formless and flat surface with a root-mean-squared (RMS) roughness of 2.64 nm. As the annealing temperature increased from 100°C to 175°C, however, the blend films were more phase-separated, displayed larger surface aggregates, domains were clearly present, and the RMS roughness increased from 3.22 nm to 4.81 nm. These aggregated domains most likely originated from the enhanced

intermolecular interactions³¹ among the **DTBDT-TTPD** molecules, as indicated by the optical properties. A higher surface roughness is expected to increase the internal light scattering and enhance light absorption.³² Together, these characteristics of thermally annealed films were expected to increase the J_{sc} value and efficiency of the **DTBDT-TTPD:PC₇₁BM** devices relative to the device prepared without annealing.

Nanostructural order

Insights into the molecular packing of the copolymer films were obtained by examining the XRD patterns (out-of-plane) of the **DTBDT-TTPD:PC₇₁BM** films prepared using different thermal annealing procedures (Fig. 6). As expected, the XRD diffraction studies indicated that the **DTBDT-TTPD:PC₇₁BM** films prepared without thermal annealing exhibited relatively weak crystalline structures with a defined diffraction signal (100) at $2\theta = 2.90^\circ$ that corresponded to a d -spacing distance of 21.16 Å. A signal at $2\theta = 5.80^\circ$ was also detected, corresponding to scattering from a second-order reflection. Both diffraction peaks remained at the same position as the annealing temperature was increased, but the intensities gradually increased and the peaks were narrowed. Further increases in the annealing temperatures increased the intensity of the third-order diffraction peak, indicating the presence of long-range crystallite ordering. These results suggested that the thermal annealing treatment should improve the crystalline stacking structure,³³ in good agreement with the AFM images. The high-order crystallites in the blend film enabled efficient charge transport,³⁴ which explained why the thermally annealed devices showed an almost 10% higher PCE and superior performances compared to the solar cells prepared without thermal annealing.

Charge carrier mobility

We further investigated the effects of thermal annealing on the charge transport properties of

the active layers using the space charge limited current (SCLC) method. The experimental details are described in the Experimental Section. As shown in Fig. 7 and Table 3, films prepared without annealing exhibited very low hole and electron mobilities of $5.54 \times 10^{-6} \text{ cm}^2 \text{ V}^{-1} \text{ S}^{-1}$ and $3.58 \times 10^{-7} \text{ cm}^2 \text{ V}^{-1} \text{ S}^{-1}$, respectively; however, thermal annealing significantly enhanced the charge carrier mobilities in the **DTBDT-TTPD**:PC₇₁BM devices (from $9.17 \times 10^{-6} \text{ cm}^2 \text{ V}^{-1} \text{ S}^{-1}$ to $8.29 \times 10^{-5} \text{ cm}^2 \text{ V}^{-1} \text{ S}^{-1}$ for hole mobility (μ_h) and from $8.11 \times 10^{-7} \text{ cm}^2 \text{ V}^{-1} \text{ S}^{-1}$ to $3.24 \times 10^{-5} \text{ cm}^2 \text{ V}^{-1} \text{ S}^{-1}$ for electron mobility (μ_e)). The above analysis indicated that (1) the excellent photovoltaic properties of **DTBDT-TTPD** arose mainly from the small molecule's superior charge transport abilities. The fully planar molecular geometry of **DTBDT-TTPD** favored the ordered molecular packing in the condensed state,³⁵⁻³⁶ especially after thermal annealing treatment. The high carrier mobility that resulted from thermal annealing permitted charge carriers to travel faster during the charge transport process, resulting in a high current density.³⁷ The benefits of the high hole mobility could be realized in devices prepared with thermal annealing, as they exhibited better device performances. Moreover, the device processed from thermal annealing shows relatively well balanced mobility ($\mu_h/\mu_e = 2.6$) compared to the as-cast device ($\mu_h/\mu_e = 15.7$). The more balanced mobility contributes to higher J_{SC} and FF because the accumulated space charge limited current (SCLC) charges and hence recombination processes are reduced by the increase in the carrier mobility and enhanced charge collection efficiency.³⁸

Conclusions

In summary, a new A-D-A small molecule based on a dithienobenzodithiophene donor unit at the center and thienopyrroledione acceptor units at the terminal ends, **DTBDT-TTPD**, was successfully synthesized and found to be a promising donor for use in solution-processable OSCs. These new **DTBDT-TTPD** molecules displayed excellent thermal stability, strong

absorption, relatively low HOMO levels, and superior charge transport properties with a high hole mobility. The favorable highly ordered π -stacked structures formed by thermal annealing yielded solution-processed OSCs composed of **DTBDT-TTPD** and PC₇₁BM with a high PCE of 4.98%, a V_{OC} of 0.85 V, a J_{SC} of 10.6 mA/cm², and a FF of 56.0%. These OSCs also delivered a rarely observed 10% improvement in the PCE compared to the untreated film. A PCE exceeding 4.9% is among the highest yet reported for fully solution-processed photovoltaic devices based on DTBDT motifs. This work demonstrates that small molecules based on the DTBDT moiety present a good strategy for developing novel photovoltaic small molecule-based donor materials with a high J_{sc} and efficiency for the preparation of high-efficiency OSCs.

Experimental section

Materials

All solvents and reagents were purchased from Aldrich, Alfa Aesar, and TCI. The catalysts used in the coupling reactions were purchased from Umicore. All other materials were common commercial-grade and were used as received. All solvents were purified prior to use.

Synthesis of the small molecules

Synthesis of 5,10-bis(4,5-didecylthiophen-2-yl)benzo[1,2-b:4,5-b']dithieno[3,2-b]thiophene (1).

5,10-Bis(4,5-didecylthiophene-2-yl)benzo[1,2-b;4,5-b']diithieno[3,2-b]thiophene was prepared according to the procedure reported in the literature.¹⁵ To a 250 mL nitrogen-purged flask was added, dropwise, n-butyl lithium (2.5 M in hexane, 84.4 mmol, 33 mL) was added dropwise to a solution of 5,10-bis(4,5-didecylthiophene-2-yl)benzo[1,2-b;4,5-b']diithieno[3,2-b]thiophene (27.20 g, 74.80 mmol) in THF (100 mL) at 0°C. The mixture

was then warmed to 50°C and stirred for 2 h. 5,10-Dihydrobenzo[1,2-b:4,5-b']dithieno[3,2-b]thiopheneophen-5,10-dione (DTBD)¹³ (8.30 g, 25 mmol) was added to the reaction mixture, which was then stirred for 1 h at 50°C. The reaction mixture was cooled to ambient temperature, a mixture of SnCl₂·2H₂O (22.40 g, 100 mmol) in 10% HCl (60 mL) was added, and the mixture was stirred for 1 h. The mixture was poured into ice water and extracted with diethyl ether. The combined organic phases were concentrated to obtain the crude product. The crude product was purified by column chromatography on silica gel using hexane. The compound was further purified by recrystallization from ethanol. mp: 85–86.1°C. Yield: 31.2% as a pale yellow solid. ¹H NMR (300 MHz, CDCl₃): δ 7.47-7.45 (d, 2 H), 7.31-7.29 (d, 2 H), 7.12 (s, 2 H), 2.93-2.70 (m, 8 H), 2.17-2.15 (m, 8 H), 1.60-1.41 (m, 56 H), 0.92-0.89 (m, 12 H); ¹³C NMR (75 MHz, CDCl₃): δ 143.8, 143.4, 142.3, 139.7, 139.6, 134.4, 132.8, 131.4, 130.7, 130.2, 124.7, 120.5, 32.77, 32.71, 31.61, 30.49, 30.43, 30.37, 30.23, 30.15, 30.06, 29.07, 28.78, 23.47, 14.63; EI, MS m/z: 1027 (M⁺)

Synthesis of 2,7-bis(trimethylstannyl)-5,10-bis(4,5-didecylthiophen-2-yl)benzo[1,2-b:4,5-b']dithieno[3,2-b]thiophene (2).

The *n*-butyl lithium (2.5 M in hexane, 2.14 mmol, 0.85 mL) was added to a solution of 5,10-bis(4,5-didecylthiophen-2-yl)benzo[1,2-b:4,5-b']dithieno[3,2-b]thiophene (1) (2.0 g, 1.94 mmol) in THF (60 mL) at 0°C under nitrogen in a purged flask. The mixture was then warmed to 50°C and stirred for 2 h. Subsequently, trimethyltin chloride (1.0 M in THF, 4.28 mL, 4.28 mmol) was added, and the mixture was stirred for 3 h. The mixture was poured into ice water. The mixture was then extracted in diethyl ether, and the combined organic phase was concentrated to obtain compound (2). Further purification was carried out by recrystallization from hexane and isopropyl alcohol. mp: 104–105.3°C. Yield: 75.0% as a

light yellow solid. ^1H NMR (300 MHz, CDCl_3): δ 7.32 (s, 2 H), 7.13 (s, 2 H), 2.96-2.67 (m, 8 H), 1.83-1.73 (m, 8 H), 1.49-1.31 (m, 56 H), 0.92-0.88 (m, 12 H), 0.50-0.31 (m, 18 H); EI, MS m/z (%): 1353 (100, M^+)

Synthesis of 5-octyl-1, 3-di(thiophen-2-yl)-4H-thieno[3,4-c]pyrrole-4,6(5H)-dione (3).

1,3-Dibromo-5-octyl-4H-thieno[3,4-c]pyrrole-4,6(5H)-dione was prepared according to the procedures reported in the literature.¹⁸ 1,3-Dibromo-5-octyl-4H-thieno[3,4-c]pyrrole-4,6(5H)-dione (7.50 g, 17.73 mmol) and trimethyl(thiophen-2-yl)stannane (16.53 g, 44.32 mmol) were dissolved in 300 mL toluene in a pressure tube. The solution was degassed under nitrogen flow for 30 min. $\text{Pd}(\text{PPh}_3)_2\text{Cl}_2$ (0.37 g, 0.53 mmol) was then added to the solution. The tube was capped and heated to 110°C overnight. The mixture was extracted with dichloromethane. The organic layers were combined and dried over anhydrous MgSO_4 . After removing the solvent, the residue was purified by column chromatography on silica gel using hexane/dichloromethane (4:1) as the eluent. Recrystallization from hexanes afforded compound 3 (4.88 g, 11.34 mmol, 64%) as a yellow solid. mp: 95.3-96.1°C ^1H NMR (300 MHz, CDCl_3): δ = 8.00 (s, 2H), 7.45 (s, 2H), 7.15 (t, 2H), 3.68(t, 2H), 1.72 (m, 2H), 1.32 (m, 10H), 0.88 (t, 3H).

Synthesis of 1-(5-bromothiophen-2-yl)-5-octyl-3-(thiophen-2-yl)-4H-thieno[3,4-c]pyrrole-4,6(5H)-dione (4).

To a solution of 1-(5-bromothiophen-2-yl)-5-octyl-3-(thiophen-2-yl)-4H-thieno[3,4-c]pyrrole-4,6(5H)-dione (3) (5.50 g, 12.79 mmol) in 100 mL DMF and 100 mL CHCl_3 was added, dropwise, NBS (2.27 g, 12.79 mmol) over a period of 60 min. After 2 h, the reaction mixture was poured into water and extracted three times with chloroform. The organic phases were combined and dried over anhydrous magnesium sulfate. After removing the solvent, the

crude product was purified by column chromatography using dichloromethane/hexane (1:4) as an eluent. Recrystallization from hexanes afforded compound (4). mp: 106.5–108.3°C Yield: 53% (3.44 g, 6.78 mmol) as a yellow solid. ^1H NMR (300 MHz, DMSO): δ = 7.99 (s, 1H), 7.83 (s, 1H), 7.70 (t, 1H), 7.35 (d, 1H), 7.24(d, 1H), 3.51(t, 2H), 1.50 (s, 2H), 1.27 (m, 10H), 0.84 (m, 3H).

Synthesis of DTBDT-TTPD (5).

2,7-Bis(trimethylstannyl)-5,10-bis(4,5-didecylthiophen-2-yl)benzo[1,2-b:4,5-b']dithieno[3,2-b] thiophene (2) (0.60 g, 0.44 mmol) and 1-(5-bromothiophen-2-yl)-5-octyl-3-(thiophen-2-yl)-4H-thieno[3,4-c]pyrrole-4,6(5H)-dione (4) (0.50 g 0.98 mmol) were dissolved in toluene (18 mL). Pd(PPh₃)₄ (0.03 g, 0.026 mmol) was added to the mixture, which was then heated at 110°C and stirred for 48 h. The reaction mixture was poured into methanol (200 mL) and filtered over a glass filter. The crude product was further purified by Soxhlet extraction with ethyl acetate and chloroform. The chloroform solution containing the product was reprecipitated in methanol and filtered. Yield: 52% (0.43 g, 0.25mmol). mp > Td ^1H NMR (300 MHz, CDCl₃)[ppm] δ = 7.96 (d, 2H), 7.80 (d, 2H), 7.40 (d, 2H), 7.21 (s, 2H), 7.08 (m, 4H), 6.94 (d, 2H), 3.65 (t, 4H), 2.97 (t, 4H), 2.72 (t, 4H), 1.88-1.65 (br, 12H), 1.54-1.25 (br, 76H), 0.91-0.83 (br, 18H). ^{13}C NMR (500 MHz, CDCl₃): δ 162.33, 142.94, 141.52, 140.38, 139.82, 139.42, 139.39, 138.55, 135.99, 135.61, 133.06, 132.49, 131.83, 131.04, 130.91, 130.54, 129.82, 129.65, 128.53, 128.38, 128.23, 124.40, 123.49, 116.6, 38.59, 32.10, 31.98, 31.81, 31.17, 29.88, 29.81, 29.79, 29.69, 29.66, 29.51, 29.44, 29.24, 29.21, 28.56, 28.51, 28.21, 27.06, 22.71, 22.62, 14.10, 14.04, MS (MALDI-TOF/TOF) : calculated for C₁₀₆H₁₃₂N₂O₄S₁₂, 1880.68; Found, 1882.5

General Measurements

¹H-NMR spectra were recorded using a Bruker AM-200 spectrometer. ¹³C-NMR spectra were measured on a Bruker Advance-300 spectrometer. HRMS (EI) spectra were collected using a high-resolution GC mass spectrometer with a LabRAM HR800 UV. Mass (MALDI-TOF/TOF) spectra were determined using a high-resolution 4800 Tof/Tof mass spectrometer with Voyager DE-STR. Thermal gravimetric analysis (TGA) was performed on a TA TGA 2100 thermogravimetric analyzer under purified nitrogen with a heating rate of 10°C/min. Differential scanning calorimetry (DSC) was conducted under nitrogen on a TA Instruments 2100 DSC. The sample was heated at 10°C/min from 30 to 300°C. The UV-Vis absorption spectra were determined using a Cary 5000 UV-vis-near-IR double beam spectrophotometer. Photoluminescence (PL) spectra were obtained using a FP-6500 (JASCO). Cyclic voltammetry (CV) was performed using a PowerLab/AD instrument model system in a 0.1 M tetrabutylammonium hexafluorophosphate (Bu₄NPF₆) solution in anhydrous acetonitrile as the supporting electrolyte, at a scan rate of 50 mV/s. A glassy carbon disk (~0.05 cm²) coated with a thin small molecule film, an Ag/AgCl electrode, and a platinum wire were used as the working electrode, reference electrode, and counter electrode, respectively. Density functional theory (DFT) calculations were carried out at the B3LYP/6-31G* level of theory using Gaussian 09 computational programs. The atomic force microscope (AFM) (Multimode IIIa, Digital Instruments) was operated in tapping mode to obtain surface images (surface area: 5 × 5 μm²) of the small molecule:PC₇₁BM blend films after thermal annealing under ambient conditions. The X-ray diffraction (XRD) spectra were collected at the 5A beamline (wavelength = 1.071 Å) at the Pohang Accelerator Laboratory (PAL) in Korea. The small molecule:PC₇₁BM blended films were prepared on a Si/PEDOT:PSS substrate using the spin-coating method.

Fabrication and characterization of the small molecule solar cells

The devices were fabricated using a conventional structure: glass/ITO/PEDOT:PSS/active layer(**DTBDT-TTPD**:PC₇₁BM)/LiF/Al, using a solution process. The ITO-coated glass substrates were cleaned by ultrasonic treatment in detergent, deionized water, acetone, and isopropyl alcohol under ultrasonication for 20 min each, followed by drying under a nitrogen stream. A thin layer (~40 nm) of PEDOT:PSS (Clevios P VP AI 4083, filtered at 0.45 μm PVDF) was spin-coated at 4000 rpm onto the ITO surface. After baking at 120°C for 20 min, the substrates were transferred into a nitrogen-filled glovebox. Subsequently, the active layer was spin-coated from the donor–acceptor blend solutions in different ratios, concentrations, and thicknesses. Finally, a 0.8 nm LiF layer and an 80 nm Al layer were deposited onto the active layer under high vacuum (2×10^{-6} Torr). The effective area of each cell was 9 mm², as defined by the mask. The current density-voltage (*J-V*) characteristics of the photovoltaic devices were measured under ambient conditions using a Keithley Model 2400 source-measurement unit. An Oriel xenon lamp (450 W) with an AM 1.5 G filter was used as the solar simulator. The light intensity was calibrated to 100 mW/cm² using a silicon cell with a KG5 filter, calibrated by the National Renewable Energy Laboratory (LREL). The EQE spectra were obtained using a photomodulation spectroscopic set-up (model Merlin, Oriel), a calibrated Si UV detector, and a SR570 low noise current amplifier.

Hole and electron mobility measurements

The hole-only devices were fabricated in the structure: ITO/PEDOT:PSS/**DTBDT-TTPD**:PC₇₁BM/Au. The Au layer was deposited at low speed (1 /s) to avoid the penetration of Au atoms into the active layer. We also fabricated electron-only devices with the architecture Al/**DTBDT-TTPD**:PC₇₁BM/Al. The device characteristics were extracted by modeling the dark current under an applied forward bias. The mobilities were extracted by

fitting the current–voltage curves using the Mott–Gurney relationship (space charge limited current).

$$J = \frac{9}{8} \epsilon_0 \epsilon_r \mu_h \frac{V^2}{L^3},$$

where J is the current density, L is the film thickness of the active layer, μ_h is the hole mobility, ϵ_r is the relative dielectric constant of the transport medium, ϵ_0 is the permittivity of free space, V is the internal voltage in the device, and $V = V_{\text{appl}} - V_r - V_{\text{bi}}$, where V_{appl} is the voltage applied to the device, V_r is the voltage drop due to the contact resistance and series resistance across the electrodes, and V_{bi} is the built-in voltage due to the relative work function difference between the two electrodes. V_{bi} could be determined from the transition between the ohmic region and the SCLC region.

Acknowledgements

This work was supported by the New & Renewable Energy of the Korea Institute of Energy Technology Evaluation and Planning (KETEP), funded by the Korean Government Ministry of Knowledge Economy (No. 20123010010140).

† **Electronic supplementary information (ESI) available.** See DOI:~

Notes and references

- 1 G. Li, R. Zhu and Y. Yang, *Nat. Photonics*, 2012, **6**, 155.
- 2 J. You, L. Dou, K. Yoshimura, T. Kato, K. Ohya, T. Moriarty, K. Emery, C. –C. Chen, J. Gao, G. Li and Y. Yang, *Nat. Comm*, 2012, **4**, 1446.
- 3 A. Mishra and P. Bäuerle, *Angew. Chem. Int. Ed.* 2012, **51**, 2020.
- 4 Y. Sun, G. C. Welch, W. L. Leong, C. J. Takacs, G. C. Bazan and A. J. Heeger, *Nat. Mater*,

2012, **11**, 44.

5 B. Walker, A. B. Tamayo, X. –D. Dang, P. Zalar, J. H. Seo, A. Garcia, M. Tantiwivat and T. –Q. Nguyen, *Adv. Funct. Mater.* 2009, **19**, 3063.

6 Y. Liu, C. –C. Chen, Z. Hong, J. Gao, Y. Yang, H. Zhou, L. Dou, G. Li and Y. Yang, *Scientific Reports*, 2013, **3**, 3356.

7 H. Zhou, L. Yang and W. You, *Macromolecules* 2012, **45**, 607.

8 T. S. van der Poll, J. A. Love, T. –Q. Nguyen and G. C. Bazan, *Adv. Mater.* 2012, **24**, 3646.

9 P. M. Beaujuge and J. M. J. Fréchet, *J. Am. Chem. Soc.* 2011, **133**, 20009.

10 L. Biniek, B. C. Schroeder, J. E. Donaghey, N. Y-Gross, R. S. Ashraf, Y. W. Soon, C. B. Nielsen, J. R. Durrant, T. D. Anthopoulos and I. McCulloch, *Macromolecules*, 2013, **46**, 727.

11 H. Bronstein, R. S. Ashraf, Y. Kim, A. J. P. White, T. Anthopoulos, K. Song, D. James, W. Zhang, I. McCulloch, *Macromol. Rapid. Commun.* 2011, **32**, 1664.

12 H. J. Son, L. Lu, W. Chen, T. Xu, T. Zheng, B. Carsten, J. Strzalka, S. B. Darling, L. X. Chen and L. Yu, *Adv. Mater.* 2013, **25**, 838.

13 Y. Wu, Z. Li, X. Guo, H. Fan, L. Huo and J. Hou, *J. Mater. Chem.*, 2012, **22**, 21362.

14 J. E. Anthony, *Chem. Rev.* 2006, **106**, 5028.

15 H. –J. Yun, Y. –J. Lee, S. –J. Yoo, D. S. Chung, Y. –H. Kim and S. –K. Kwon, *Chem. Eur. J.* 2013, **19**, 13242.

16 Y. Wu, Z. Li, W. Ma, Y. Huang, L. Huo, X. Guo, M. Zhang, H. Ade and J. Hou, *Adv. Mater.* 2013, **25**, 3449.

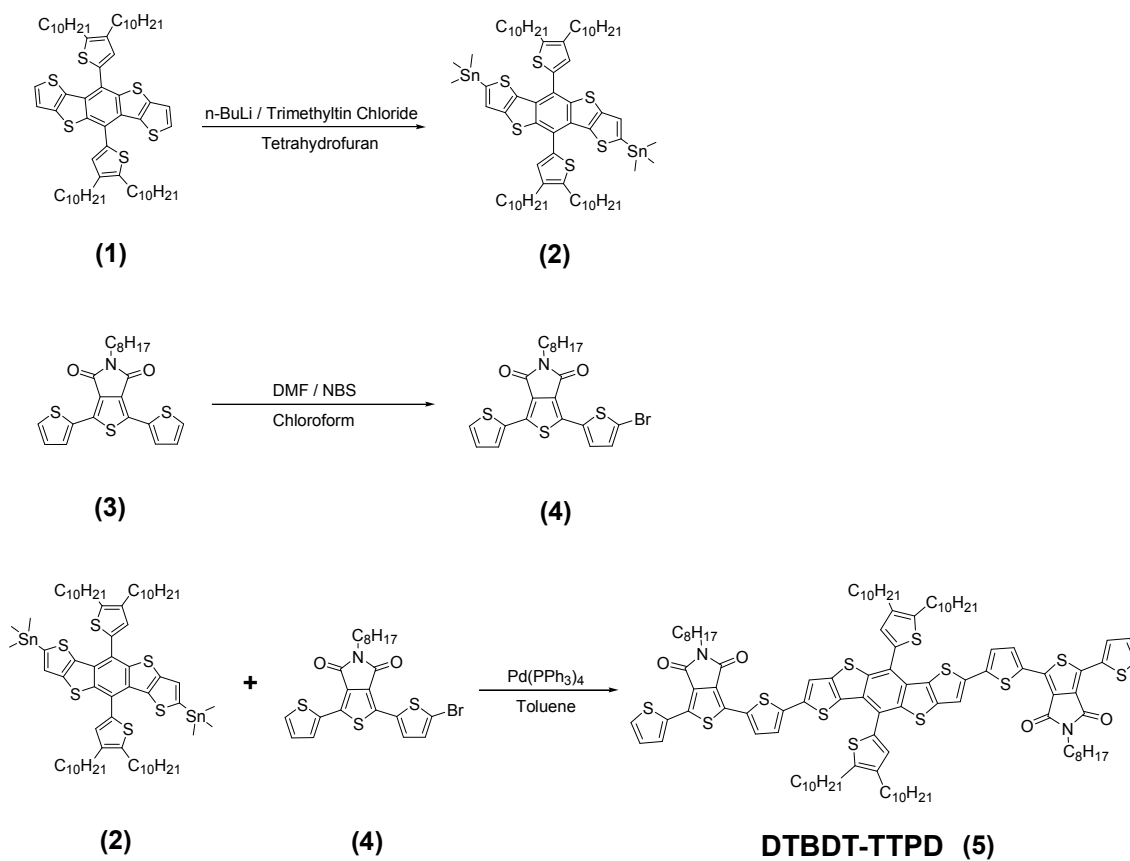
17 Y. Zou, A. Najari, P. Berrouard, S. Beaupre, B. R. Aich, Y. Tao and M. Leclerc, *J. Am. Chem. Soc.* 2010, **132**, 5330.

18 J. Ha, Y. J. Kim, J. Park, T. K. An, S. –K. Kwon, C. E. Park and Y. –H. Kim, *Chem. Asian J.* 2014, **9**, 1045.

19 Y. Lin, P. Cheng, Y. Liu, X. Zhao, D. Li, J. Tan, W. Hu, Y. Li and X. Zhan, 2012, **99**, 301.

- 20 J. Yuan, Z. Zhai, H. Dong, J. Li, Z. Jiang, Y. Li and W. Ma, *Adv. Funct. Mater.* 2013, **23**, 885.
- 21 Y. Li, K. Yao, H. –L. Yip, F. –Z. Ding, Y. –X. Xu, X. Li, Y. Chen and A. K. –Y. Jen, *Adv. Funct. Mater.* 2014, DOI: 10.1002/adfm.201303953.
- 22 R. Shivanna, S. Shoaee, S. Dimitrov, S. K. Kandappa, S. Rajaram, J. R. Durrant and K. S. Narayan, *Energy Environ. Sci.*, 2014, **7**, 435.
- 23 J. Huang, C. Zhan, X. Zhang, Y. Zhao, Z. Lu, H. Jia, B. Jiang, J. Ye, S. Zhang, A. Tang, Y. Liu, Q. Pei and J. Yao, *ACS Appl. Mater. Interfaces*, 2013, **5**, 2033.
- 24 J. Peet, J. Y. Kim, N. E. Coates, W. L. Ma, D. Moses, A. J. Heeger and G. C. Bazan, *Nat. Mater.*, 2007, **6**, 497.
- 25 L. Fu, W. Fu, P. Cheng, Z. Xie, C. Fan, M. Shi, J. Ling, J. Hou, X. Zhan and H., Chen, *J. Mater. Chem. C*, 2014, DOI: 10.1039/c3ta13534a.
- 26 L. Dou, J. You, J. Yang, C. –C. Chen, Y. He, S. Murase, T. Moriarty, K. Emery, G. Li and Y. Yang, *Nat. Photonics.*, 2012, **6**, 180.
- 27 V. Gupta, A. K. K. Kyaw, D. H. Wang, S. Chand, G. C. Bazan and A. J. Heeger, *Scientific Reports*, 2013, **3**, 1965.
- 28 Zhou H, Yang L and Y Wei, *Macromolecule*, 2012, **45**, 607.
- 29 S. H. Park, A. Roy, S. Beaupre, S. Cho, N. Coates, J. S. Moon, D. Moses, M. Leclerc, K. Lee and A. J. Heeger, *Nat. Photonics*, 2009, **3**, 297.
- 30 J. Seifer, Y. Sun and A. J. Heeger, *Adv. Mater.* **2014**, DOI: 10.1002/adma.201305160.
- 31 A. K. K. Kyaw, D. H. Wang, C. Luo, Y. Cao, T. –Q. Nguyen, G. C. Bazan and A. J. Heeger, *Adv. Energy Mater.*, 2014, 1301469.
- 32 J. D. Zimmerman, X. Xiao, C. K. Renshaw, S. Wang, V. V. Diev, M. E. Thompson, S. R. Forrest, *Nano. Lett.* 2012, **12**, 4366.
- 33 J. Huang, H. Jia, L. Li, Z. Lu, W. Zhang, W. He, B. Jiang, A. Tang, Z. Tan, C. Zhan, Y. Li,

- J. Yao, *Phys. Chem. Chem. Phys.* 2012, **14**, 14238.
- 34 D. H. Kim, A. L. Ayzner, A. L. Appleton, K. Schmidt, J. Mei, M. F. Toney, Z. Bao, *Chem. Mater.* **2013**, *25*, 431.
- 35 H. Bronstein, E. Collado-Fregoso, A. Hadipour, Y. W. Soon, Z. Huang, S. D. Dimitrov, R. S. Ashraf, B. P. Rand, S. E. Watkins, P. S. Tuladhar, L. Meager, J. R. Durrant and I. McCulloch, *Adv. Funct. Mater.*, 2013, **23**, 5647.
- 36 I. Meager, R. S. Ashraf, S. Rossbauer, H. Bronstein, J. E. Donaghey, J. Marchall, B. C. Schroeder, M. Heeney, T. D. Anthopoulos and I. McCulloch, *Macromolecules* 2013, **46**, 5961.
- 37 J. Gao, L. Dou, W. Chen, C. -C. Chen, X. Guo, J. You, B. Bob, W. -H. Chang, J. Strzalka, C. Wang, G. Li and Y. Yang, *Adv. Energy. Mater.*, 2014, **4**, 1300739.
- 38 Y. Lin, Y. Li and X. Zhan, *Adv. Energy. Mater.*, 2013, **3**, 724.



Scheme 1. Synthetic route to preparing an A-D-A-type small molecule, **DTBDT-TTPD**.

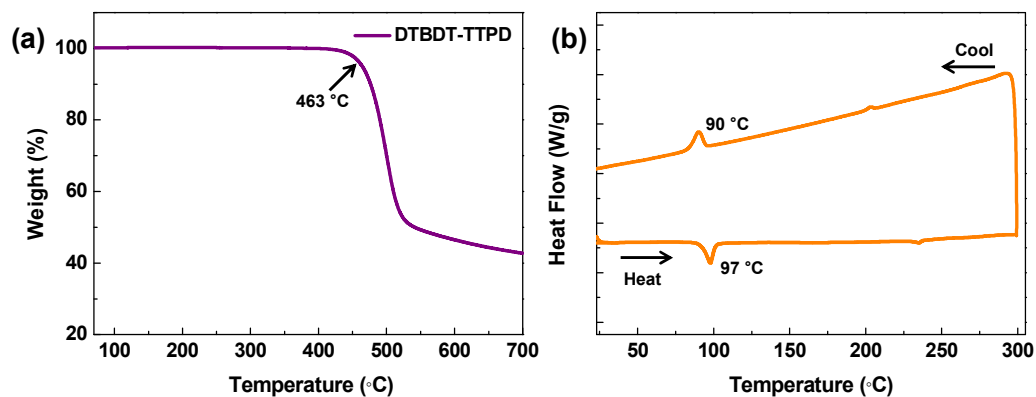


Fig. 1 (a) TGA trace obtained from **DTBDT-TTPD**, at a heating rate of $10^{\circ}\text{C min}^{-1}$. (b) The DSC curve of the **DTBDT-TTPD**, obtained at a heating rate of $10^{\circ}\text{C min}^{-1}$.

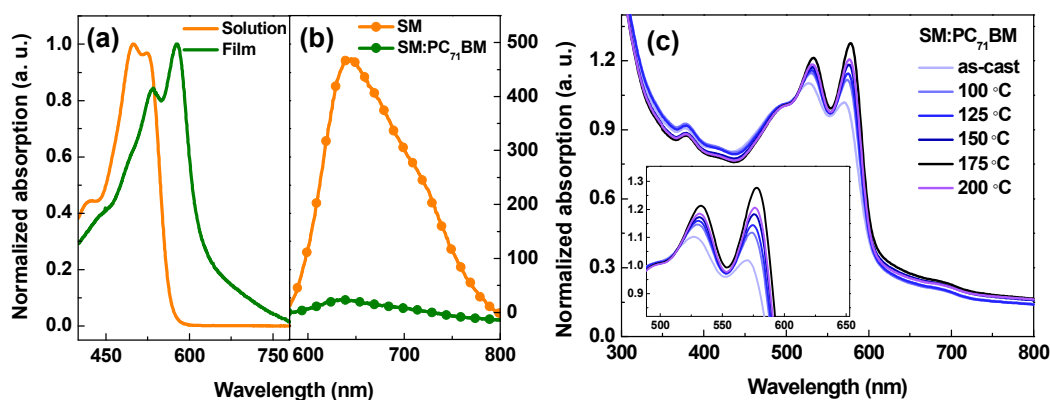


Fig. 2 (a) UV-vis absorption spectra of the pure **DTBDT-TTPD**, in the solution and film states; (b) PL spectra of a **DTBDT-TTPD** and **DTBDT-TTPD:PC₇₁BM** (1:2) blend film; and (c) the absorption spectra of the blended **DTBDT-TTPD** films (1:2, weight ratio), prepared at various temperatures.

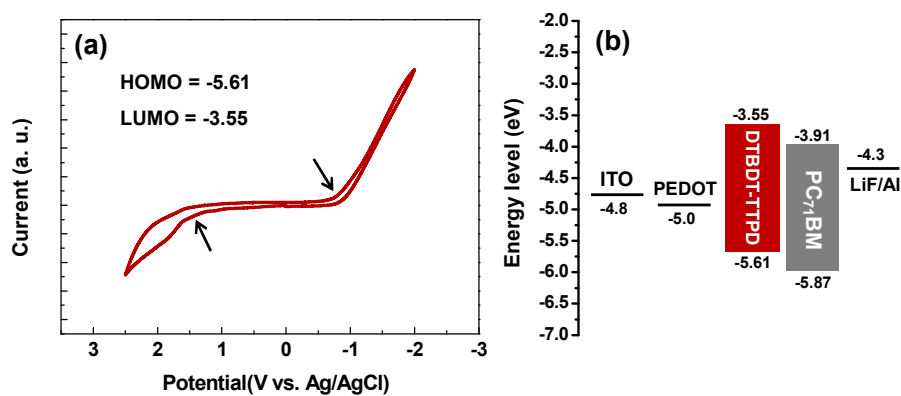


Fig. 3 (a) Cyclic voltammograms of DTBDT-TTPD, and (b) energy levels of the different components in the photovoltaic device.

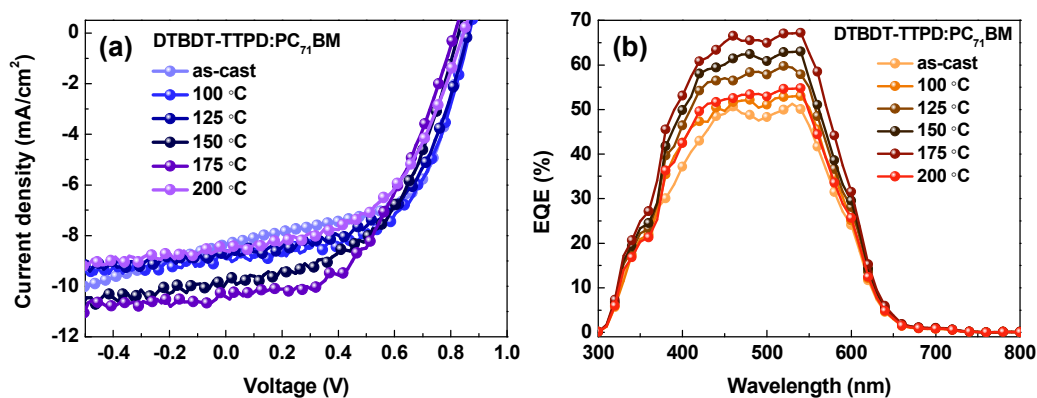


Fig. 4 (a) Light $J-V$ characteristics of DTBDT-TTPD:PC₇₁BM solar cells prepared at various annealing temperatures; and (b) External quantum efficiency (EQE) spectra of the corresponding devices prepared at various temperatures.

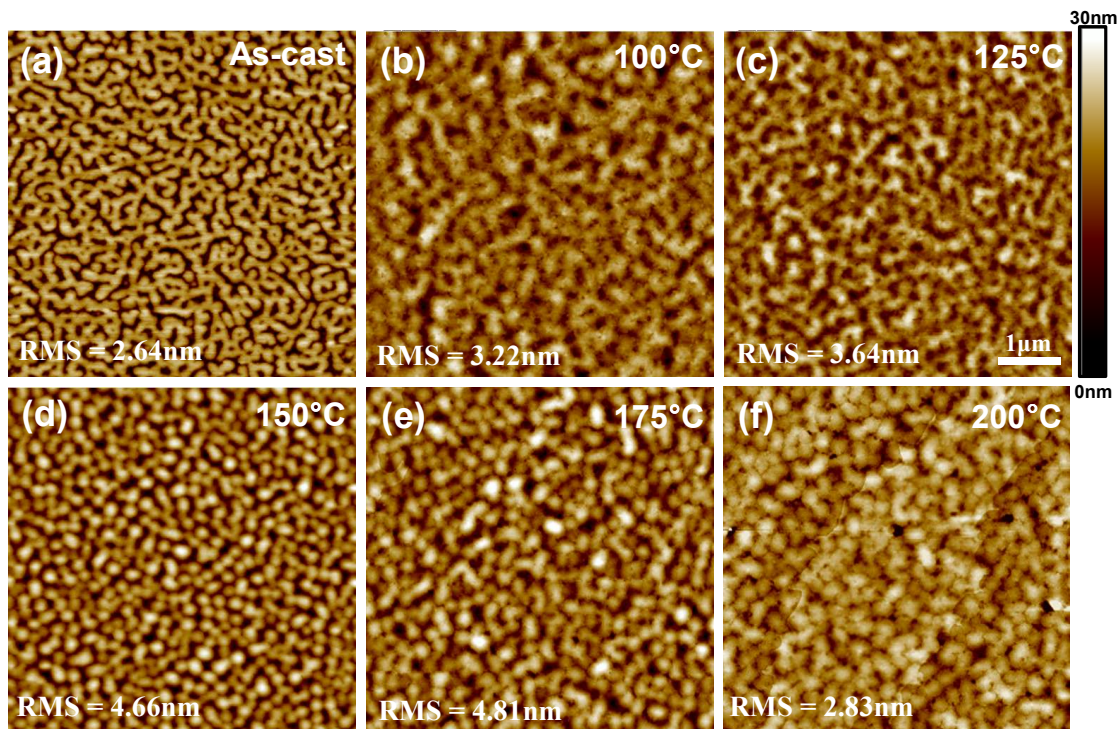


Fig. 5 AFM height images of DTBDT-TTPD:PC₇₁BM blend films as a function of the annealing temperature.

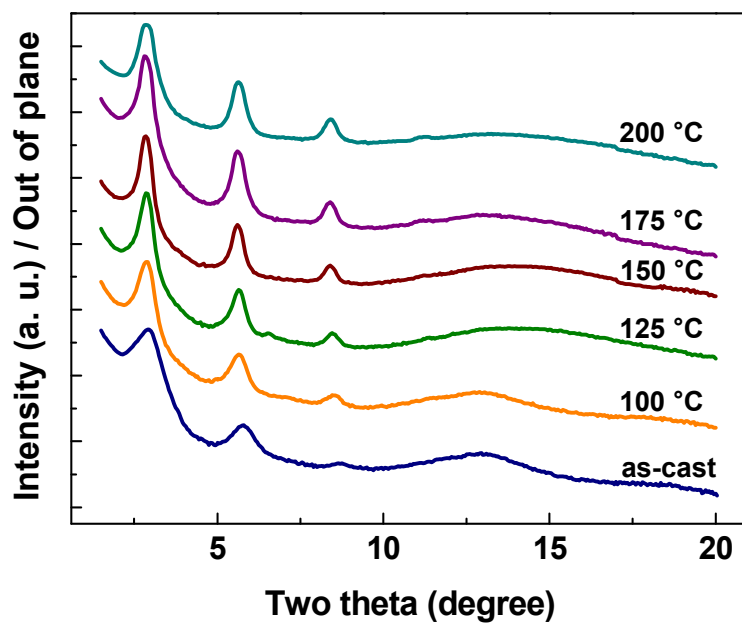


Fig. 6 XRD patterns obtained from the DTBDT-TTPD:PC₇₁BM blend films (1:2 w/w) prepared at various annealing temperatures.

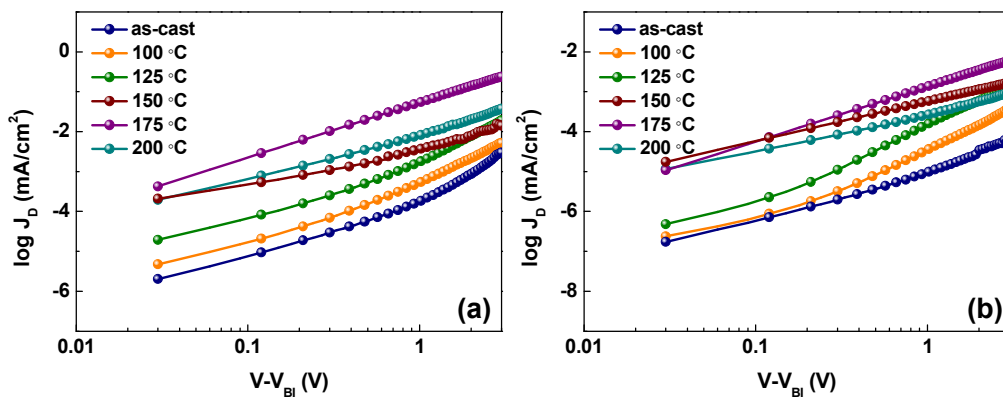


Fig. 7 Current-voltage (J - V) characteristics of (a) hole only and (b) electron only devices at a various annealing temperatures in the dark.

Table 1. Optical and electrochemical properties of **DTBDT-TTPD**.

Small Molecule	λ_{\max} (nm) solution	λ_{\max} (nm) film	λ_{onset} (nm) film	E_g^{opt} (eV) ^a	$E_{\text{onset}}^{\text{ox}}$ (eV)	$E_{\text{onset}}^{\text{red}}$ (eV)	E_{HOMO} (eV)	E_{LUMO} (eV)
DTBDT-TTPD	498, 524	532, 577	657	1.88	1.25	-0.81	-5.61	-3.55

Table 2. Summary of the photovoltaic properties of **DTBDT-TTPD:PC₇₁BM** BHJ solar cell devices annealed at various temperatures.

Small molecule : PCBM	Annealing Temperature (°C)	V_{oc} (V)	J_{sc} (mA / cm ²)	FF (%)	PCE (%)
	as	0.86	8.4	54.8	3.95
	100	0.87	8.5	55.3	4.09
	125	0.87	8.9	55.8	4.32
DTBDT-TTPD:PC₇₁BM	150	0.86	10.0	53.2	4.57
	175	0.85	10.6	56.0	4.98
	200	0.86	8.9	53.6	4.05

Table 3. Summary of the hole and electron mobilities of **DTBDT-TTPD:PC₇₁BM** films prepared by different annealing temperatures.

Active layer	Solvent/ active layer thickness (nm)	Annealing Temperature (°C)	μ_h (cm ² /V s)	μ_e (cm ² /V s)	μ_h/μ_e
DTBDT-TTPD:PC₇₁BM	CF / 85	as	5.54×10^{-6}	3.58×10^{-7}	15.7
	CF / 85	100	9.17×10^{-6}	8.11×10^{-7}	11.3
	CF / 85	125	3.24×10^{-5}	3.52×10^{-6}	9.2
	CF / 85	150	5.01×10^{-5}	1.06×10^{-5}	4.7
	CF / 85	175	8.29×10^{-5}	3.24×10^{-5}	2.6
	CF / 85	200	6.23×10^{-5}	1.22×10^{-5}	5.1